Blockade of HERG Channels Expressed in *Xenopus laevis* Oocytes by External Divalent Cations

Won-Kyung Ho,* Injune Kim,# Chin O. Lee,# Jae Boum Youm,* Suk Ho Lee,* and Yung E. Earm*
*Department of Physiology, Seoul National University College of Medicine, Seoul 110-799, and #Department of Life Science, Pohang University of Science and Technology, Pohang 790-784, Republic of Korea

ABSTRACT We have investigated actions of various divalent cations (Ba^{2+}, Sr^{2+}, Mn^{2+}, Co^{2+}, Ni^{2+}, Zn^{2+}) on human ether-a-go-go related gene (HERG) channels expressed in *Xenopus laevis* oocytes using the voltage clamp technique. All divalent cations inhibited HERG current dose-dependently in a voltage-dependent manner. The concentration for half-maximum inhibition (K_i) decreased at more negative potentials, indicating block is facilitated by hyperpolarization. K_i at 0 mV for Zn^{2+}, Ni^{2+}, Co^{2+}, Ba^{2+}, Mn^{2+}, and Sr^{2+} was 0.19, 0.36, 0.50, 0.58, 2.36, and 6.47 mM, respectively. The effects were manifested in four ways: 1) right shift of voltage dependence of activation, 2) decrease of maximum conductance, 3) acceleration of current decay, and 4) slowing of activation. However, each parameter was not affected by each cation to the same extent. The potency for the shift of voltage dependence of activation was in the order $Zn^{2+} > Ni^{2+} \geq Co^{2+} > Ba^{2+} > Mn^{2+} > Sr^{2+}$, whereas the potency for the decrease of maximum conductance was $Zn^{2+} > Ba^{2+} > Sr^{2+} > Co^{2+} > Mn^{2+}$. The kinetics of activation and deactivation were also affected, but the two parameters are not affected to the same extent. Slowing of activation by Ba^{2+} was most distinct, causing a marked initial delay of current onset. From these results we concluded that HERG channels are nonselectively blocked by most divalent cations from the external side, and several different mechanism are involved in their actions. There exist at least two distinct binding sites for their action: one for the voltage-dependent effect and the other for reducing maximum conductance.

INTRODUCTION

The human *ether-a-go-go* related gene (HERG), has recently been found to encode a voltage-gated K^+ channel with properties nearly identical to a cardiac delayed rectifier K^+ current, I_{Kr} (Sanguinetti et al., 1995; Trudeau et al., 1995). I_{Kr} plays a fundamental role in cardiac excitability by contributing to repolarization and thereby regulating action potential duration (Noble and Tsien, 1969; Sanguinetti and Jurkiewicz, 1991). In sinoatrial node cells of the heart, the decay of I_{Kr} also contributes to pacemaker depolarization (Brown et al., 1976; Brown and DiFrancesco, 1980; Irisawa et al., 1993). Tissue distribution study shows that the *erg*-related gene is abundant in a wide variety of tissues, suggesting that it plays an important role in other tissues (Wymore et al., 1997). The functional role of HERG channels in noncardiac tissues is not yet fully understood. Recently, it has been shown that HERG encodes an inward rectifying K^+ channel (I_{IR}) in a variety of tumor cell lines, and a role of I_{IR} in neoplastic transformation and cell proliferation was suggested (Arcangeli et al., 1997; Bianchi et al., 1998). The same group had previously observed that in neuroblastoma cells resting membrane potential (V_{REST}) is much lower and varies widely (−40–10 mV) compared to normal cells, and found that the scattering of V_{REST} correlates with the scattering of the voltage dependence of I_{IR} (Arcangeli et al., 1995). These results indicate that the biophysical property of I_{IR} is responsible for determining the characteristic feature of V_{REST}.

Although HERG belongs a family of voltage-dependent K^+ channels, its electrophysiological characteristics are quite distinct from those of other voltage-dependent K^+ channels. A fully activated current-voltage relationship shows strong inward rectification, and its mechanism has been investigated by many authors, showing that it is attributable to a rapid voltage-dependent inactivation mechanism (Shibasaki, 1987; Smith et al., 1996; Spector et al., 1996). However, the activation mechanism has not been investigated widely, but was considered in general not to be different from that of other voltage-dependent channels. Recent studies have shown that the voltage dependence of the HERG channel activation is affected sensitively by the concentration of external Ca^{2+} and Mg^{2+}. The same observation had been made for I_{Kr} in sinoatrial cells (Ho et al., 1996), and for I_{IR} in neuronal cells (Faravelli et al., 1996). From these reports it can be proposed that the high sensitivity of the voltage dependence of activation to external Ca^{2+} and Mg^{2+} is one of characteristic features that distinguish the HERG channel from classical inward rectifier channels. Ho et al. (1998) interpreted this effect by using a voltage-dependent block model originally proposed by Woodhull (1973), and suggested that the voltage dependence of HERG in physiological conditions is mainly determined by the voltage dependence of the channel block by Ca^{2+}, rather than by the intrinsic gating whose voltage dependence lies at very negative potentials (Zou et al., 1997). However, it has still not been determined whether this effect is specific to Ca^{2+} and Mg^{2+}. In the present study

Received for publication 27 July 1998 and in final form 30 December 1998.
Address reprint requests to Won-Kyung Ho, M.D., Ph.D., Department of Physiology, Seoul National University College of Medicine, Yonkeun-Dong, Chongno-Ku, Seoul 110-799, Republic of Korea. Tel.: 82-2-7408227; Fax: 82-2-7639667; E-mail: wonkyung@plaza.snu.ac.kr.

0006-3495/99/04/1959/13 $2.00

we investigated the effect of various divalent cations (Ba^{2+}, Sr^{2+}, Mn^{2+}, Co^{2+}, Ni^{2+}, Zn^{2+}) on the activation of HERG, and found that all of them modify HERG channel activation, but with different characteristics. We have evaluated various possible mechanisms in the Discussion.

METHODS

Expression of HERG in oocytes

Complementary RNA of HERG was synthesized by in vitro transcription from 1 μg of linearized cDNA using T7 mMessage mMachine kits (Ambion, Austin, TX) and stored in 10 mM Tris-HCl (pH 7.4) at −80°C. Stage V–VI oocytes were surgically removed from female *Xenopus laevis* (Nasco, Modesto, CA) anesthetized with 0.17% tricaine methanesulfonate (Sigma). Following suture, frogs were allowed to recover in isolation in a tank. Theca and follicle layers were manually removed from the oocytes by using fine forceps. Oocytes were then injected with 40 nl cRNA (0.1–0.5 μg/μl). After injection, oocytes were maintained in modified Barth's solution containing (in mM): 88 NaCl, 1 KCl, 0.4 $CaCl_2$, 0.33 $Ca(NO_3)_2$, 1 $MgSO_4$, 2.4 $NaHCO_3$, 10 HEPES (pH 7.4), supplemented with 50 μg ml^{-1} gentamicin sulfate. Currents were studied 2–7 days after injection.

Solutions and voltage clamp recording from oocytes

Ringer's solution contained (in mM): 96 NaCl, 2 KCl, 0.5 $CaCl_2$, and 5 HEPES (pH adjusted to 7.4 with NaOH). The concentrations of $BaCl_2$, $NiCl_2$, $SrCl_2$, $MnCl_2$, $CoCl_2$, $NiCl_2$, and $ZnCl_2$ were varied as indicated in each experiment without changing the concentration of other chemicals. Currents were measured at room temperature (21–23°C) with a two-electrode voltage clamp amplifier (Warner Instrument, Hamden, CT). Electrodes were filled with 3 M KCl and had a resistance of 2–4 MΩ for voltage-recording electrodes and 0.6–1 MΩ for current-passing electrodes. Stimulation and data acquisition were controlled with Digidata and pCLAMP software (Axon Instruments, Foster City, CA).

RESULTS

HERG currents (I_{HERG}) expressed in *Xenopus* oocytes were recorded in 2 mM $[K^+]_o$ Ringer's solution. External Ca^{2+} concentration was kept at 0.5 mM, since nonselective leak conductance of oocytes increases if divalent cations are totally absent. Throughout the experiments, the holding potential was adjusted between −60–80 mV to obtain the minimum leak current, but the repolarization potential was made constant at −60 mV. As shown in Fig. 1 *A*, depolarizing pulses from a holding potential of −70 mV induced time-dependent increases of outward I_{HERG}. The amplitude of outward I_{HERG} was measured at the end of a 5-s pulse (I_{ss}) and plotted against test potentials in Fig. 1 *B*. I_{ss} grew larger as the membrane was depolarized, and then decreased progressively with further depolarization due to rapid inactivation of HERG current, resulting in a bell-shaped *I-V* relationship with its peak at −30 mV. On repolarizing to −60 mV, outward tail currents (I_{tail}) developed (Fig. 1 *A*). The amplitude of I_{tail} increased progressively as increasing the amplitude of depolarizing pulses. The amplitude of I_{tail} was normalized relative to the amplitude obtained at +20 mV test pulse, and plotted against the test potential in Fig. 1 *C* (*filled squares*). Continuous curves were drawn by fitting the data with the Boltzmann equation, and half-activation voltages ($V_{1/2}$) were obtained. We considered that this plot can represent the voltage dependence of HERG channel activation, although a 5-s pulse was not enough to induce a steady state activation, especially at potentials near threshold where the time course of activation was very slow. When a longer pulse (10 s) was applied, $V_{1/2}$ slightly shifted to the left, but the shift caused by prolonging the pulse duration was not >5 mV. We considered this error as acceptable, and used 5-s pulses throughout the subsequent experiments.

When Ba^{2+} was added to the bath solution, the amplitudes of HERG current decreased in a dose-dependent manner. The effect of various concentrations of $[Ba^{2+}]_o$ on I_{ss} is demonstrated in Fig. 1 *B*. As $[Ba^{2+}]_o$ was progressively increased, the I_{ss}-*V* relationship shifted to the right and the amplitude of I_{ss} decreased. The decrease of I_{ss} by Ba^{2+} was voltage-dependent: 0.5 mM Ba^{2+} reduced I_{ss} by 80.5 ± 4.3% at −40 mV, 67.6 ± 7.1% at −30 mV, 51.6 ± 8.6% at −20 mV, and 31.4 ± 9.6% at −10 mV (n = 5). I_{ss} at more positive potentials was not significantly affected by increasing Ba^{2+}, but a slight increase was observed. Since HERG current was mostly inactivated at this potential (Fig. 2), we regarded this effect as not being due to the change of HERG current, but to a gradual increase of nonspecific leak current during the course of experiments.

The I_{tail}-*V* curve, which is generally regarded as representing the voltage-dependent activation property of HERG current, was also significantly affected by $[Ba^{2+}]_o$ (Fig. 1 *C*). It shifted progressively to the right as $[Ba^{2+}]_o$ increased, and the maximum I_{tail} obtained after large depolarization was also reduced very significantly. These results indicate that as $[Ba^{2+}]_o$ is increased, larger depolarization is needed for the activation of HERG channel, and the fully activated conductance induced by a sufficient depolarization is also reduced.

To examine whether the change of maximum I_{tail} represents the change of maximum conductance of HERG currents, fully activated current-voltage relationships were obtained by using a double-pulse protocol: a varying level of test pulses following the prepulse to +20 mV, which is given to induce a full activation (Fig. 2). The amplitude of the current at the beginning of test pulses was measured at its peak when inactivation was removed, but deactivation had not yet progressed. The fully activated current-voltage relationship showed a strong inward rectification with a negative slope conductance, which is a well-known characteristic of HERG channels caused by rapid inactivation (Smith et al., 1996; Spector et al., 1996). The increase of $[Ba^{2+}]_o$ decreased the fully activated conductance in a dose-dependent manner. There was no shift in fully activated *I-V* relationships and no change in reversal potentials.

For further analysis, the chord conductance was obtained from the fully activated current-voltage relationship. It was normalized to the maximum slope conductance at each

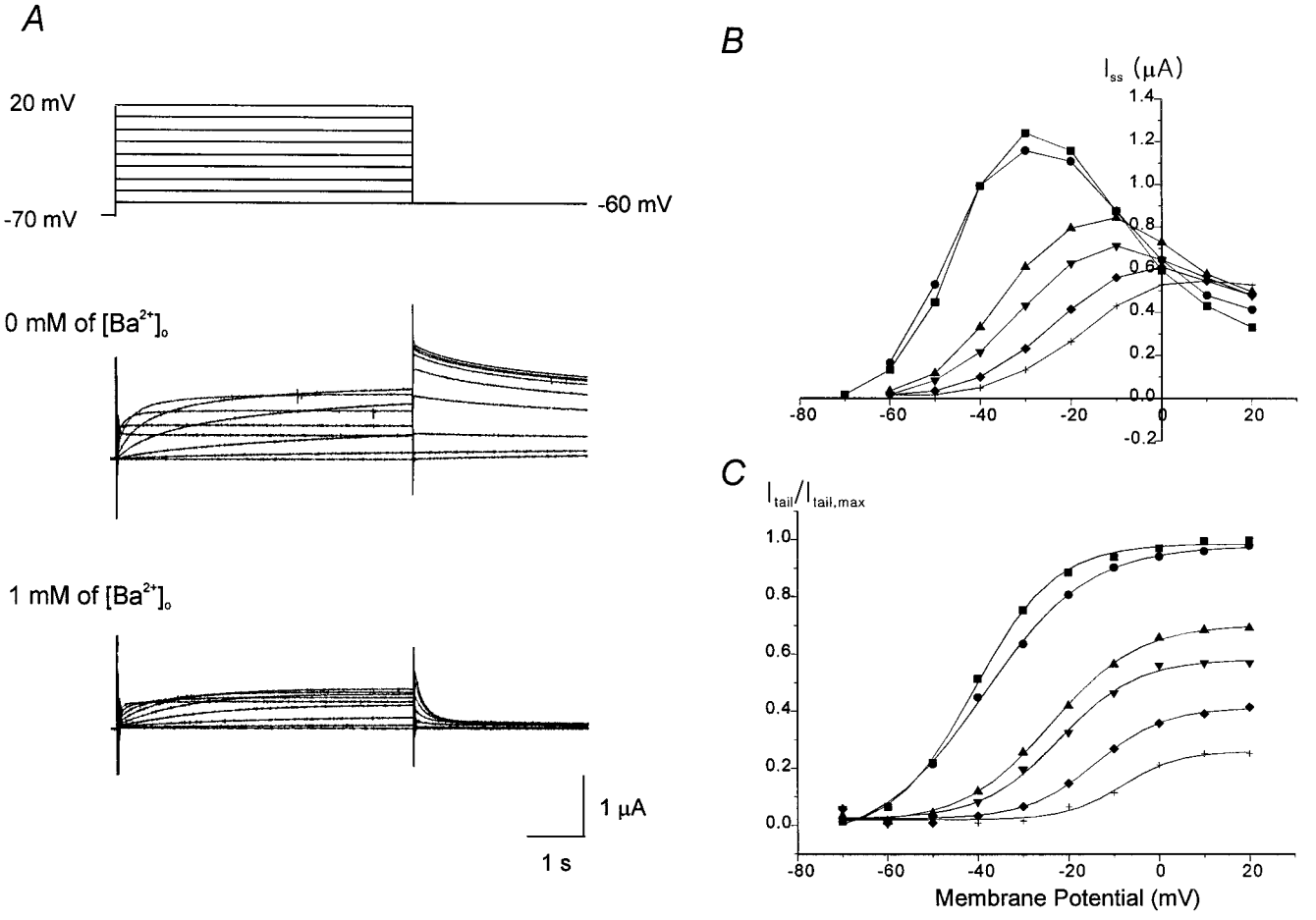

FIGURE 1 Effect of external Ba^{2+} concentration on HERG currents elicited by depolarizing voltage pulses. (*A*) Superimposed current traces elicited by depolarizing voltage pulses (5 s) in 10-mV steps (*top panel*) from a holding potential of −70 mV in 0 mM (*middle panel*) and in 1 mM $[Ba^{2+}]_o$ (*bottom panel*). $[K^+]_o$ is 2 mM. (*B*) Plot of the steady-state current measured at the end of depolarizing pulses against the pulse potential in different external $[Ba^{2+}]_o$ (obtained from the same cell shown in *A*. (*C*) Plot of the normalized tail current measured at its peak just after repolarization. Similar observations from three more cells. Symbols in *B* and *C*: 0 mM (■), 0.05 mM (●), 0.5 mM (▲), 1 mM (▼), 2.0 mM (♦), 5 mM (+). Lines in *C* are the fits to the Boltzmann equation, $y = 1/\{1 + \exp((-V + V_{1/2})/dx)\}$ ($V_{1/2}$ from left to right; −43.1 mV, −41.8 mV, −25.5 mV, −21.9 mV, −14.0 mV, −8.1 mV).

concentration of $[Ba^{2+}]_o$, and plotted in Fig. 2 *B*. This could be an estimation of inactivation, and $V_{1/2}$ in the absence of Ba^{2+} was −49.2 mV. This value agrees well with previous reports (−49 mV in Sanguinetti et al., 1995; −45 mV in Wang et al., 1997). It was shifted slightly to the right by increasing $[Ba^{2+}]_o$, and $V_{1/2}$ at 1 mM $[Ba^{2+}]_o$ was −45.5 mV. At higher concentrations of Ba^{2+}, rapid block by Ba^{2+} prevented the accurate measurement of the fully activated current at high negative potential, and curve-fitting was not appropriate. However, it could be noticed that data points were not far from the curve for 1 mM Ba^{2+}, suggesting that the effect of Ba^{2+} on inactivation is not as prominent as that on activation.

In Fig. 3, the dose-response relationship of Ba^{2+} block was analyzed. The relative amplitude of I_{tail} in the presence of Ba^{2+} in respect to the maximum I_{tail} in the absence of Ba^{2+} was regarded as the fraction of unblocked channels (y) in the presence of Ba^{2+} at the steady state. The dose-response relationship for the effect of $[Ba^{2+}]_o$ on y was obtained at each test potential, and plotted in Fig. 3 *A*. It could be fitted by the Hill equation as follows:

$$y = 1/(1 + [Ba^{2+}]_o^n/K_i) \quad (1)$$

Since n for the best fit was between 0.8 and 1.3, we fixed n at 1. The concentration for half-maximum inhibition, K_i, was voltage-dependent. K_i at 0 mV was 0.59 mM (obtained from the mean of four cells) and it decreased e-fold by 15.1 mV hyperpolarization (Fig. 3 *B*), suggesting that Ba^{2+} block is facilitated by hyperpolarization.

The other important feature was observed in the effect of Ba^{2+} on current kinetics. In Fig. 4 *A*, current traces evoked by depolarization to −20 mV from the holding potential of −80 mV at various $[Ba^{2+}]_o$ are shown on a different scale to compare the time course easily by adjusting each trace to have the same amplitude. The effect of Ba^{2+} on current onset was strikingly prominent. Application of 0.05 mM Ba^{2+} induced profound slowing of current activation. Furthermore, the current onset showed a significant delay, resulting in a sigmoid time course. Interestingly, further

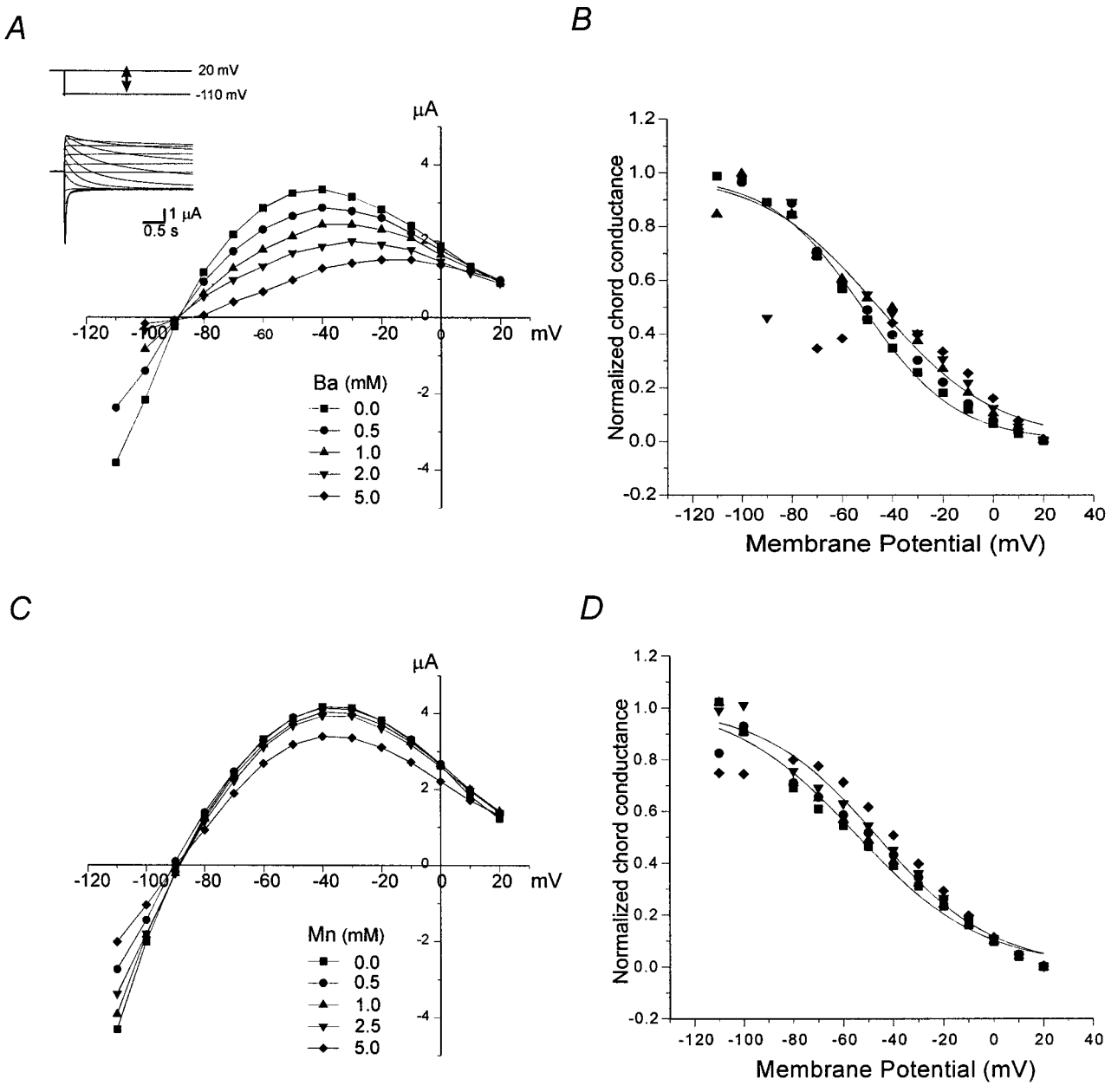

FIGURE 2 Effect of Ba^{2+} (*A, B*) and Mn^{2+} (*C, D*) on the fully activated current-voltage relationship and the inactivation curve. (*A*) *Inset:* Superimposed current traces (*lower traces*) elicited by various level of test pulses ranging from −110 to +20 mV following the prepulse to +20 mV for 5 s (*upper traces*). Peak currents measured in the beginning of test pulses were plotted against the test pulse potential in various concentrations of Ba^{2+}. Similar observations in three more cases for Ba^{2+}. (*B*) Plot of the normalized chord conductance measured from the data shown in *A*. Inactivation curves were obtained by fitting data to the Boltzmann equation. $V_{1/2}$ and slope factor (in mV) were −49.2 and 18.9 in 0 mM Ba^{2+} (*left curve*); −45.5 and 23.0 in 1 mM Ba^{2+} (*right curve*). (*C*) Same protocol as in *A* with various $[Mn^{2+}]_o$. (*D*) Same protocol as in *B* with various $[Mn^{2+}]_o$. Continuous curves are for 0 mM Mn^{2+} (*left*) and 2.5 mM Mn^{2+} (*right*).

increase of $[Ba^{2+}]_o$ produced only a little more effect. This effect is demonstrated in the plot of the reciprocal of the time constant of current activation at various $[Ba^{2+}]_o$ and various potentials (Fig. 4 *B*). The time course did not fit well with a single exponential function, suggesting that several steps may be involved in channel opening in the presence of Ba^{2+}, but the time constant was obtained using single exponential fitting in order to present the change of time course by $[Ba^{2+}]_o$ in a simple manner. However, the decay rate was generally well-fitted with a single exponential. It was proportionally increased by increasing $[Ba^{2+}]_o$ as shown in Fig. 5 *A*. The relationship between $[Ba^{2+}]_o$ and the decay rate (see Fig. 10 *A*) shows that the data are fitted with a straight line. The decay rate was plotted over wide potential range in Fig. 5 *B*, showing that it is exponentially increased by hyperpolarization.

We then tested the effect of another divalent cation belonging to the alkali metal, Sr^{2+}, on I_{HERG} using the same

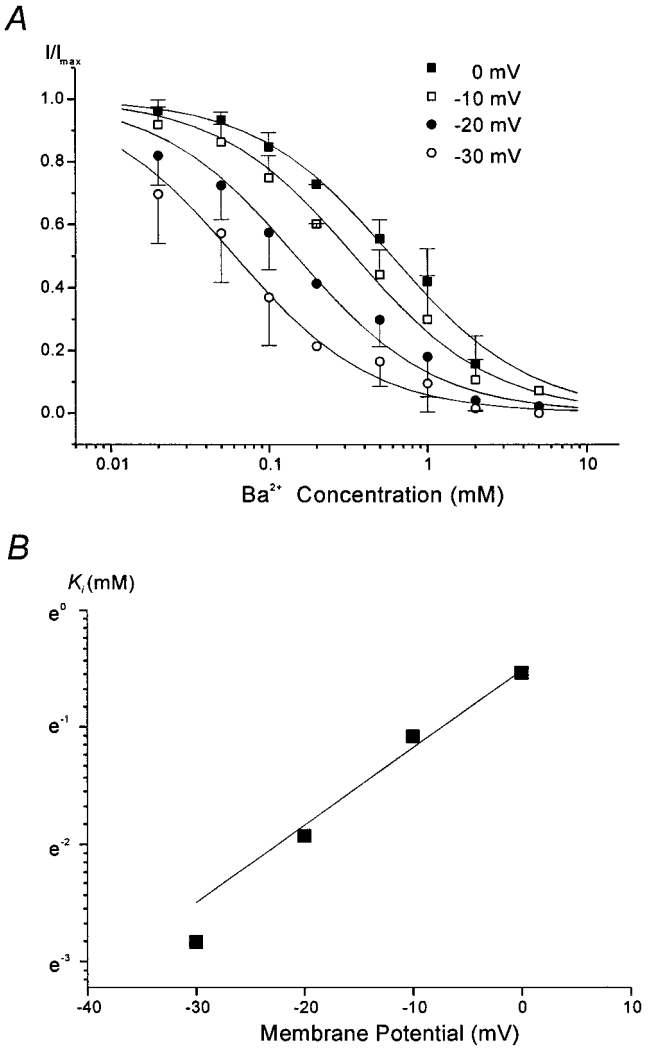

FIGURE 3 Dose-response relationship (*A*) and voltage dependence of K_i (*B*) for Ba^{2+}. (*A*) Data obtained from four cases using the same protocol as shown in Fig. 1 *C* were averaged and plotted against $[Ba^{2+}]_o$ for different potentials (−30 mV (○), −20 mV (●), −10 mV (□), and 0 mV (■)), and the curves were drawn by fitting with the Hill equation. Concentrations for half-maximum inhibition (K_i) from left to right: 0.06, 0.15, 0.34, and 0.59 mM, respectively. (*B*) Semilogarithmic plot of the concentration of Ba^{2+} for half-inhibition (K_i) against the membrane potential. K_i was obtained from the dose response curve shown in *A* at different potentials. Lines drawn by a least-square fitting. K_i decreased e-fold for 15.1 mV hyperpolarization.

experimental protocol. In Fig. 6 *A*, superimposed current traces activated by depolarization to −20 mV from the holding potential, −60 mV, were demonstrated. When $[Sr^{2+}]_o$ was increased progressively, the amplitudes of I_{HERG} decreased, but in contrast to the effect of Ba^{2+}, the rate of current activation was hardly affected by increasing $[Sr^{2+}]_o$. The amplitude of tail currents recorded upon repolarization was reduced by increasing $[Sr^{2+}]_o$, but with little change in the time course of current decay. The plot of I_{tail}-V curves (Fig. 6 *B*) showed that $V_{1/2}$ shifted to the right and maximum I_{tail} was decreased by the increase of $[Sr^{2+}]_o$. The decrease of maximum I_{tail} was more significant than the shift of $V_{1/2}$ when compared with the effect of $[Ba^{2+}]_o$. This result may suggest that shift of the voltage dependence and decrease of maximum conductance are independent phenomena.

We then tested divalent cations that belong to transitional metals Mn^{2+}, Ni^{2+}, Co^{2+}, and Zn^{2+}. In Fig. 7 *A*, superimposed current traces evoked by depolarization to −20 mV from the holding potential of −80 mV at various $[Mn^{2+}]_o$ were demonstrated. Not only the amplitude of current, but also the speed of current activation decreased. However, contrary to the effect of Ba^{2+}, initial delay of current onset was not observed. Alternatively, the tail current obtained at

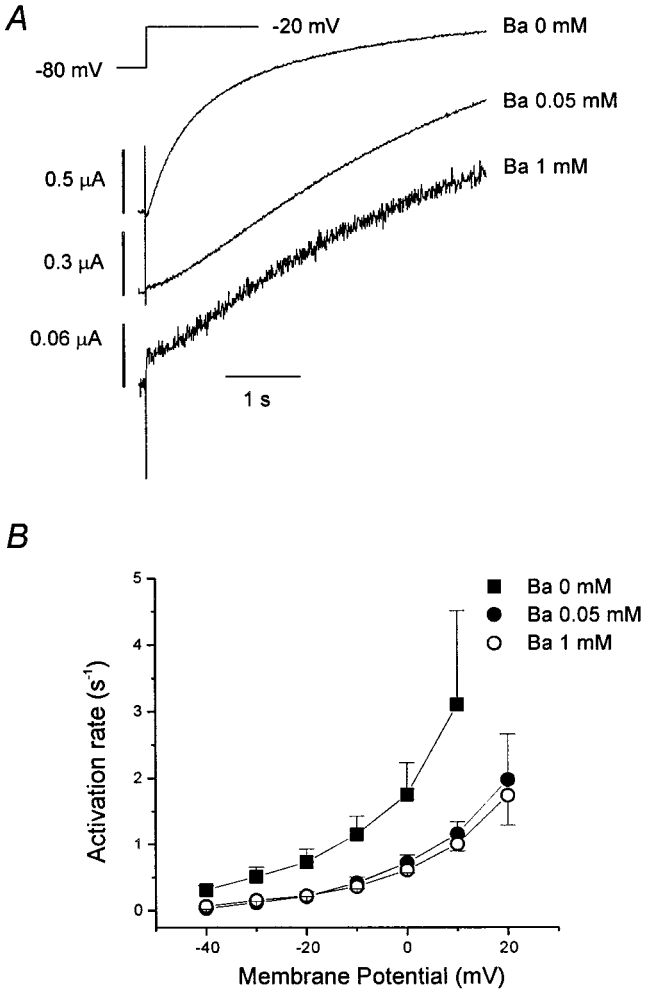

FIGURE 4 Effect of Ba^{2+} on kinetics of current onset. (*A*) Current traces evoked by depolarization to −20 mV from the holding potential of −80 mV at 0 mM, 0.05 mM, and 1 mM $[Ba^{2+}]_o$ on a different scale. Note the prominent initial delay in the presence of Ba^{2+}. (*B*) Current activation was fitted to a single exponential function, and the reciprocal of time constant was plotted against test potential. Mean ± SE obtained from four cells. $[Ba^{2+}]_o$: 0 mM (■), 0.05 mM (●), 1 mM (○). Amplitude (μA) at −40, −30, −20, −10, 0, 10, and 20 mV were 0.86 ± 0.27, 1.21 ± 0.51, 1.21 ± 0.43, 0.9 ± 0.34, 0.55 ± 0.21, 0.29 ± 0.11, and 0.08 ± 0.03 for 0 mM Ba^{2+}; 2.89 ± 1.48, 2.44 ± 0.97, 1.65 ± 0.59, 1.11 ± 0.51, 0.67 ± 0.33, 0.51 ± 0.22, and 0.29 ± 0.11 for 0.05 mM Ba^{2+}; 0.45 ± 0.16, 0.88 ± 0.44, 1.13 ± 0.68, 1.22 ± 0.79, 0.92 ± 0.73, 0.63 ± 0.54, and 0.4 ± 0.33 for 1 mM Ba^{2+}.

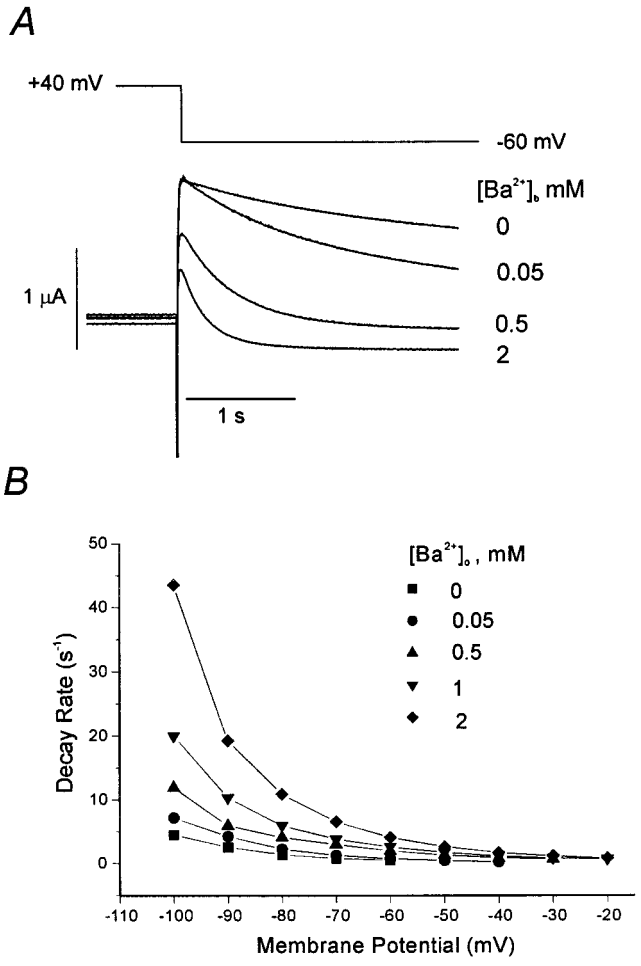

FIGURE 5 Effect of Ba^{2+} on kinetics of current decay. (*A*) Superimposed current traces recorded on repolarization to −60 mV after 5-s depolarizing pulses to +40 mV at different $[Ba^{2+}]_o$. (*B*) Current decay was fitted with single exponential functions and the reciprocal of the time constant was plotted against voltage at various $[Ba^{2+}]_o$. Symbols: 0 mM (■), 0.05 mM (●), 0.5 mM (▲), 1 mM (▼), and 2.0 mM (◆).

−60 mV after 5-s depolarization to +20 mV showed significant acceleration dose-dependently, but without a change in amplitude (Fig. 7 *B*). I_{ss}-*V* relationship obtained at various $[Mn^{2+}]_o$ is shown in Fig. 7 *C*. It shifted to the right and the amplitude of I_{ss} decreased as $[Mn^{2+}]_o$ was increased. The decrease of I_{ss} by Mn^{2+} was also voltage-dependent: 1 mM Mn^{2+} reduced I_{ss} by 90.3 ± 8.1% at −50 mV, 66.7 ± 5.0% at −40 mV, 48.3 ± 3.2% at −30 mV, and 32.4 ± 3.7% at −20 mV (n = 4). K_i of Mn^{2+} obtained using the same method shown in Fig. 3 *A* at 0 mV was 2.36 mM, indicating that Mn^{2+} is ~4 times less potent than Ba^{2+}. It decreased e-fold by 14.7 mV hyperpolarization, showing that voltage dependence is similar. I_{tail}-*V* curve also shifted progressively to the right, indicating that larger depolarization is needed for the activation of HERG channel as $[Mn^{2+}]_o$ increases (Fig. 7 *D*). However, the amplitude of the tail current evoked by large depolarization was hardly affected. It was reduced a little only at high concentration. This result suggests that Mn^{2+} hardly affected the maximum conductance, and this was confirmed in the experiment obtaining the fully activated current shown in Fig. 2 *C*. Contrary to the effect of Ba^{2+}, the effect of $[Mn^{2+}]_o$ on fully activated current was very small. The effect of Mn^{2+} on the inactivation was examined in the same way described for the Ba^{2+} effect, and the result is shown in Fig. 2 *D*. One mM Mn^{2+} caused a 3.2 mV shift, and 2.5 mM Mn^{2+} caused a 8.2 mV shift in inactivation.

In Fig. 8, the effect of Zn^{2+} is demonstrated. An increase of $[Zn^{2+}]_o$ decreased the current amplitude very signifi-

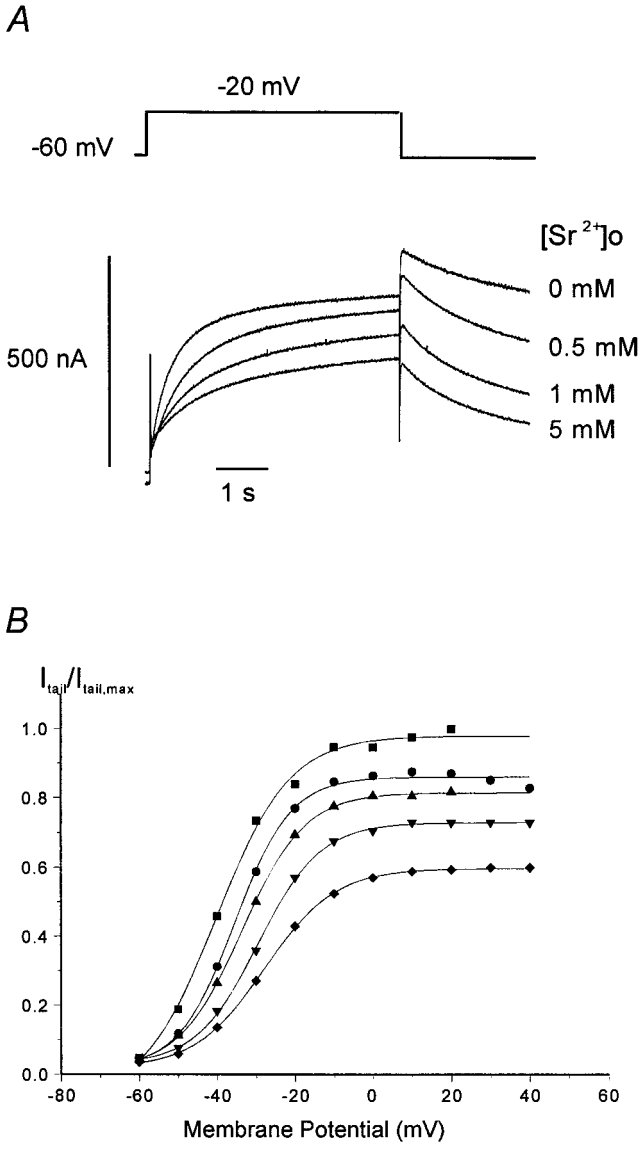

FIGURE 6 Effect of external Sr^{2+} on current activation. (*A*) Superimposed current traces elicited by depolarizing voltage pulses (5 s) to −20 mV from the holding potential of −60 mV in 0 mM, 0.5 mM, 1 mM, and 5 mM $[Sr^{2+}]_o$. (*B*) Plot of the normalized tail current measured at its peak just after repolarization from various level of depolarizing pulses. Obtained by same protocol shown in Fig. 1. Similar observations from two more cells. Symbols: 0 mM (■), 0.5 mM (●), 1 mM (▲), 2.5 mM (▼), and 5 mM (◆). Lines in *B* are the fits to the Boltzmann equation. $V_{1/2}$ from left to right; −38.6 mV, −35.8 mV, −33.9 mV, −30.3 mV, −28.4 mV).

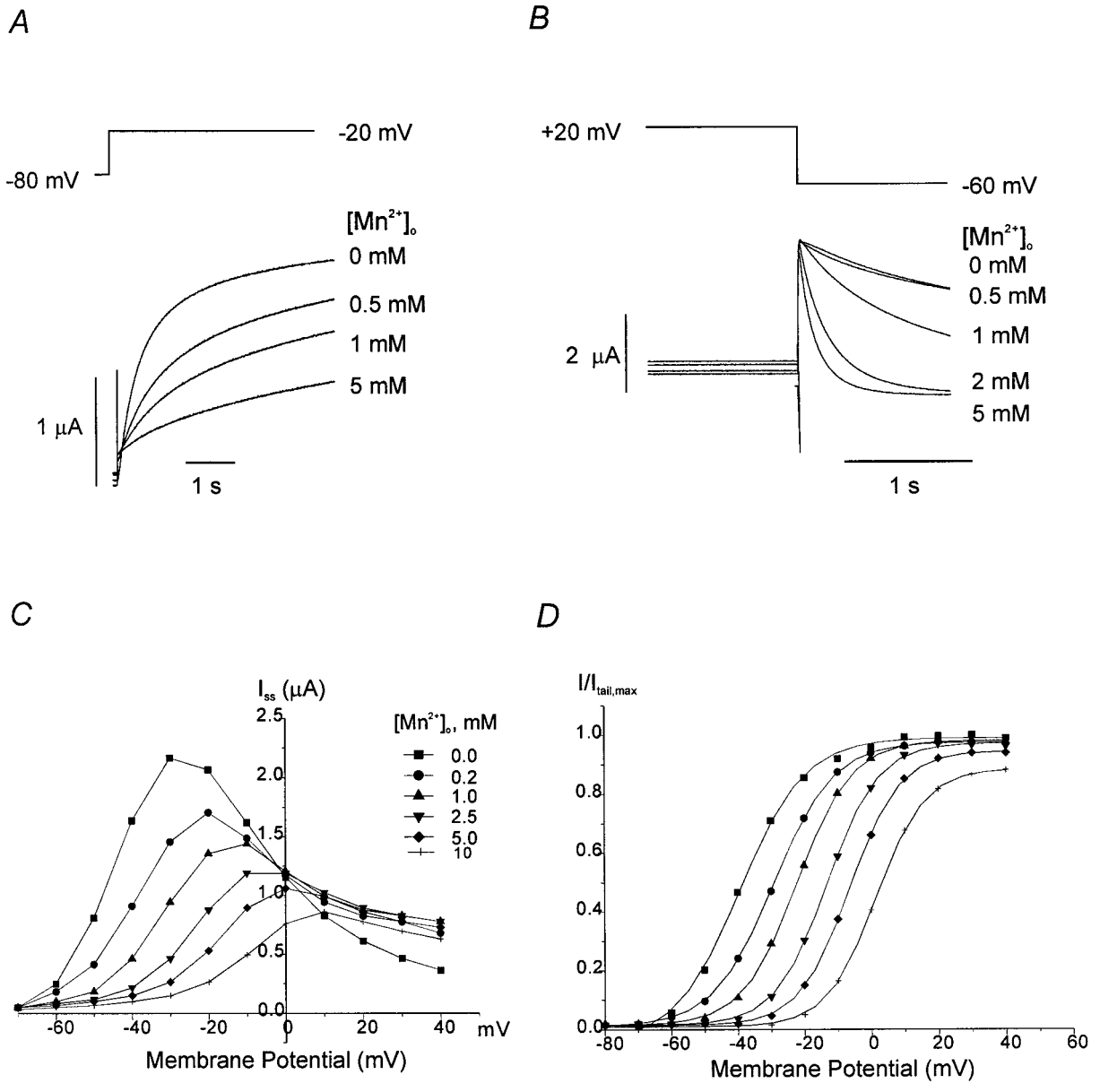

FIGURE 7 Effect of Mn^{2+}. (*A*) Superimposed current traces elicited by depolarizing voltage pulses (5 s) to −20 mV from the holding potential of −80 mV in 0 mM, 0.5 mM, 1 mM, and 5 mM $[Mn^{2+}]_o$. (*B*) Superimposed current traces recorded on repolarization to −60 mV after the pulse at +20 mV for 5 s. (*C*) Plot of the steady-state current measured at the end of depolarizing pulses (same protocol shown in Fig. 1) against the pulse potential in different external $[Mn^{2+}]_o$. (*D*) Plot of the normalized tail current measured at its peak just after repolarization. Similar observations from three more cells. Symbols in *C* and *D*: 0 mM (■), 0.2 mM (●), 1 mM (▲), 2.5 mM (▼), 5 mM (♦), 10 mM (+). Lines in *C* are the fits to the Boltzmann equation. $V_{1/2}$ from left to right; −39.4 mV, −29.2 mV, −22.2 mV, −13.2 mV, −6.4 mV, 1.4 mV.

cantly (Fig. 8, *A* and *C*). Initial delay of current onset, which was the characteristic feature of the effect of Ba^{2+}, was not significant in Zn^{2+}. In the inset of Fig. 8 *A*, currents activated at −10 mV at various $[Zn^{2+}]_o$ were normalized and superimposed to compare the time course, showing a small decrease of activation rate by increasing $[Zn^{2+}]_o$. However, the effect on the rate of current decay was very significant, and the amplitude of maximum I_{tail} was also greatly reduced by Zn^{2+} (Fig. 8 *B*). Therefore, the increase of $[Zn^{2+}]_o$ resulted in a right shift of the activation curve along with a decrease of maximum conductance (Fig. 8 *D*). K_i of Zn^{2+} at 0 mV was 0.19 mM, indicating that Zn^{2+} is the most potent among all divalent cations tested in the present study.

Effects of Ni^{2+} and Co^{2+} were also examined using the same experimental protocols. The effects of Co^{2+} were similar to those of Mn^{2+}: voltage-dependent block with a shift of activation, but with little effect on maximum conductance. K_i of Co^{2+} at 0 mV was 0.5 mM, which is about as potent as Ba^{2+}. The effect of Ni^{2+} was similar to that of Zn^{2+}: shift of activation along with a moderate decrease of maximum conductance. K_i of Ni^{2+} at 0 mV was 0.36 mM, which is more potent than Ba^{2+}, but less than Zn^{2+}.

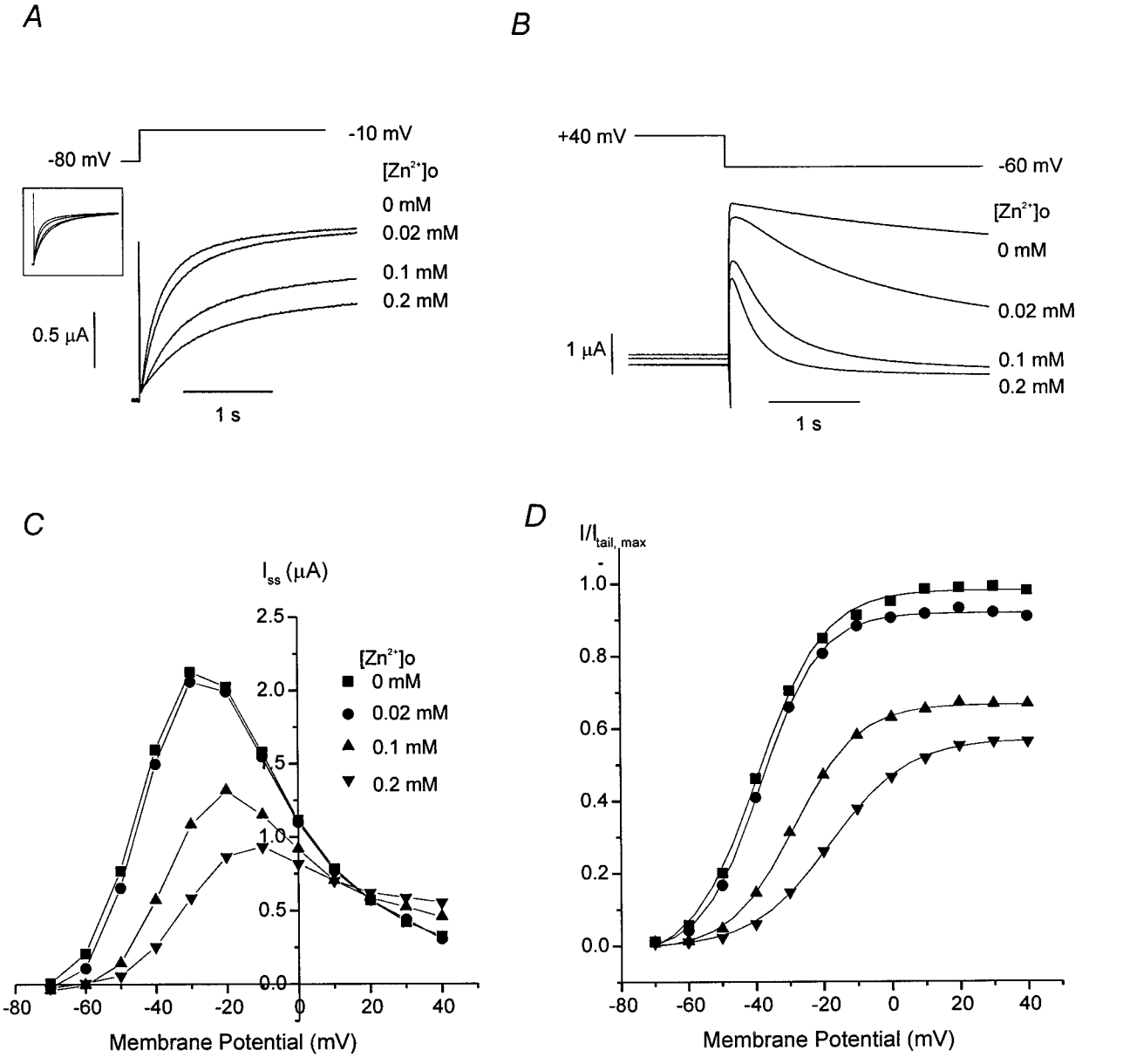

FIGURE 8 Effect of Zn^{2+}. (*A*) Superimposed current traces elicited by depolarizing voltage pulses to −20 mV from the holding potential of −80 mV in 0 mM, 0.02 mM, 0.1 mM, and 0.2 mM $[Zn^{2+}]_o$. (*B*) Superimposed current traces recorded on repolarization to −60 mV after the pulse at +40 mV for 5 s. (*C*) Plot of the steady-state current measured at the end of depolarizing pulses (same protocol shown in Fig. 1) against the pulse potential in different external $[Zn^{2+}]_o$. (*D*) Plot of the normalized tail current measured at its peak just after repolarization. Similar observations from three more cells. Symbols in *B* and *C*: 0 mM (■), 0.02 mM (●), 0.1 mM (▲), 0.2 mM (▼). Lines in *C* are the fits to the Boltzmann equation. $V_{1/2}$ from left to right; −38.2 mV, −37.7 mV, −28.2 mV, −17.7 mV.

To demonstrate the different effects of various cations on various parameters reflecting gating mechanisms of the HERG channel, we summarize the above results in the next two figures. For the parameter reflecting the effect on the voltage dependence of the channel, the shift of half-maximal activation voltage ($\Delta V_{1/2}$) is presented (Fig. 9 *A*). The effects of Sr^{2+} was the weakest of all; Mn^{2+} and Ba^{2+} are next. Zn^{2+}, Ni^{2+}, and Co^{2+} are the most potent in their effect on shifting the voltage dependence of activation.

Contrary to the effect on $V_{1/2}$, the potency of various ions for decreasing maximum conductance shows the difference in order. The relative magnitude of the maximum conductance (g_{max} in the presence of X^{2+}/g_{max} in the absence of X^{2+}) was obtained by dividing maximum tail currents (I_{tail} at +40 mV) in the presence of testing divalent cations by those in the absence of testing ions. This parameter was plotted against the concentration of various divalent cations in Fig. 9 *B*. Concentrations for half-maximum inhibition of maximum conductance, K_i, were obtained by fitting the data with Eq. 1, and they were 0.26 mM, 1.4 mM, 6.4 mM, 15.6 mM, and 72.8 mM for Zn^{2+}, Ba^{2+}, Sr^{2+}, Co^{2+}, and Mn^{2+}, respectively. The discrepancy of potency order for decreas-

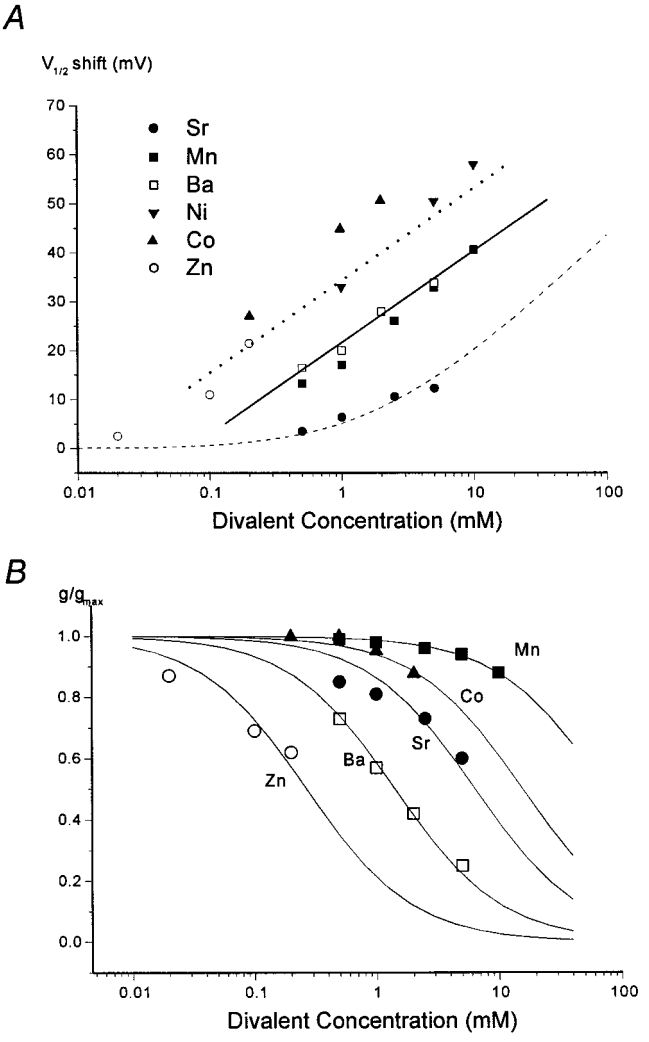

FIGURE 9 Effect of various divalent cations on the shift of the current activation (*A*) and on the decrease of maximum conductance (*B*). (*A*) Concentrations of ions on the *x* axis in log scale. Shift of $V_{1/2}$ on the *y* axis. Symbols indicate the mean of $V_{1/2}$ shift: Sr^{2+} (●, $n = 2$), Mn^{2+} (■, $n = 4$), Ba^{2+} (144, $n = 6$), Ni^{2+} (▼, $n = 2$), Co^{2+} (▲, $n = 2$), and Zn^{2+} (○, $n = 5$). *Solid straight line:* simulation result obtained from Fig. 11 *A*, assuming $k_1(0)$ of 0.068. *Dotted line:* simulation result assuming $k_1(0)$ of 0.34. *Broken curve:* simulation result assuming surface charge effect when charge density is 1/1 nm^2. (*B*) Inhibition of maximum conductance was obtained from the ratio of maximum tail current in the presence of test cations at varying concentrations to that in the absence of test cations. Continuous lines obtained by fitting with the Hill equation. K_i: 0.26 mM for Zn^{2+} (○, $n = 4$). 1.4 mM for Ba^{2+} (□, $n = 4$), 6.4 mM for Sr^{2+} (●, $n = 2$), 15.6 mM for Co^{2+} (▲, $n = 2$), and 72.8 mM for Mn^{2+} (■, $n = 4$).

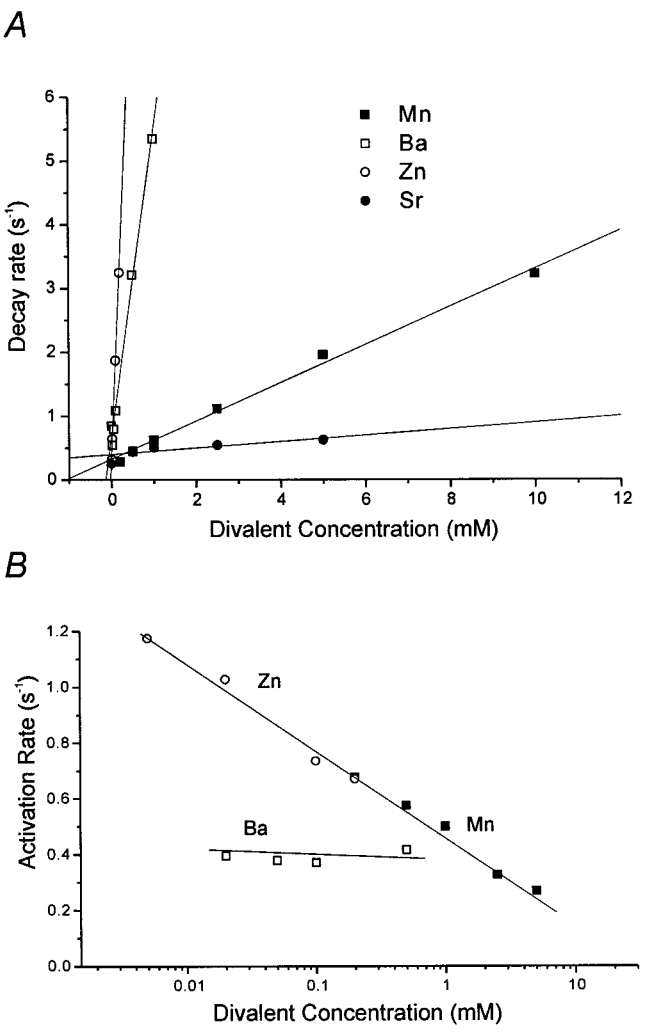

FIGURE 10 Effect of various divalent cations on the kinetics of current activation (*A*) and current decay (*B*). Obtained from one cell. (*A*) Current decay obtained at −60 mV was fitted with a single exponential function. The reciprocal of the time constant was plotted against the concentration of test cations. Straight lines are the best fits for each ion. The slopes are 14.9, 4.8, 0.29, and 0.05 mV for Zn^{2+}, Ba^{2+}, Mn^{2+}, and Sr^{2+}, respectively. (*B*) Current activation evoked by the depolarization to −20 mV was fitted with a single exponential function. The reciprocal of the time constant was plotted against the concentration of test cations.

ing maximum conductance and for shifting voltage dependence indicates that they are modulated via different mechanisms.

In Fig. 10 the rate of current decay (obtained at −60 mV) and current activation (obtained at −20 mV) are plotted against divalent concentration. For comparison, the data obtained from the same cell is demonstrated. The decay rate was proportionally increased by increasing the concentration of divalent cations, and the data were well-fitted with straight lines. The steepness was in the order $Zn^{2+} > Ba^{2+} > Mn^{2+} > Sr^{2+}$ (Fig. 10 *A*). However, the activation rate decreased with increasing concentration of divalent cations, but the effect on activation and deactivation was not equal: effects of Zn^{2+} and Mn^{2+} on current activation were similar, whereas Zn^{2+} induced a much greater effect on current deactivation than Mn^{2+}.

DISCUSSION

We have shown that all divalent cations tested in the present study inhibit HERG current in a dose-dependent manner. The effects are manifested as follows: 1) decrease of current amplitude, 2) shift of voltage dependence of activation, 3) acceleration of deactivation, 4) slowing of activation, and 5)

decrease of maximum conductance. These effects had also been observed in our previous study investigating Ca^{2+} and Mg^{2+} (Ho et al., 1996, 1998). The present study, however, has revealed that each parameter is not affected by each cation to the same extent, implying that the underlying mechanism is not a single process, but that several different pathways are involved in inhibiting HERG channels by divalent cations. Fig. 9 clearly demonstrates that the effect on $V_{1/2}$ and that on g_{max} is not equal, suggesting that two parameters are controlled by different mechanisms. These results might suggest the existence of at least two different binding sites: one for modulating the maximum conductance and one for modulating voltage-dependent gating. Fig. 10 demonstrates that the effect on activation and that on deactivation are not equal, implying that effect of divalent cations on current kinetics does not result from a simple shift of voltage dependence of gating.

Divalent cations have been one of the classical tools used to investigate gating and permeation of K^+ channels (Hille, 1992). Three mechanisms have been proposed to explain various aspects of actions of divalent cations: 1) surface charge theory, 2) voltage-dependent block theory, and 3) gating modifier theory. Although the results of the present study suggest that various mechanisms are involved in action of external divalent cations on the HERG channel, a simple scheme of the voltage-dependent block model, which has been used widely, especially to describe a voltage- and time-dependent block of various K^+ channels (Armstrong, 1971; Hagiwara et al., 1978; Standen and Stanfield, 1978; French and Shoukimas, 1985), can still explain major important features of the actions of divalent cations on HERG channels. Since the effect of Ba^{2+} has the most complicated features, we examine whether Ba^{2+} effects can be reproduced using this model. Since the inactivation process was little affected by Ba^{2+} (Fig. 2), we did not consider the inactivation process in the following simulation. The effect of Ba^{2+} producing channel blockade is described as follows:

$$\underset{(y)}{\text{Channel} + Ba^{2+}} \underset{k_{-1}}{\overset{k_1[Ba^{2+}]_o}{\rightleftharpoons}} \underset{(1-y)}{\text{Channel} - Ba^{2+}\ (\text{Blocked})}$$

In this model, acceleration of current decay on repolarization is viewed as a manifestation of channel blockade by a blocking particle. Thus, the binding rate constant, k_1, can be obtained from the time constant of current decay from the following equation.

$$\tau^{-1} = k_1[Ba^{2+}]_o + k_{-1} \quad (2)$$

The linear relationship between divalent concentrations and the rate of current decay (Fig. 10) agree well with this assumption of one-to-one binding. From the slope of this plot, k_1 can be calculated. The binding rate constant as a function of voltage can also be obtained by fitting the result in Fig. 5 *B* in the presence of 1 mM Ba^{2+}. The unbinding rate constant, $k_{-1}(V)$, was obtained from the result of Fig. 4 *B* by fitting the activation rate in the presence of 1 mM Ba^{2+}. $k_1(V)$ and $k_{-1}(V)$ can be expressed as follows:

$$k_1(V) = 0.068*\exp(-V/17) \quad (3)$$

$$k_{-1}(V) = 0.6*\exp(V/20) \quad (4)$$

We then calculate the fraction of unbound channel (y) at steady state from $k_1(V)$ and $k_{-1}(V)$ in the presence of various concentrations of Ba^{2+} using the following equation:

$$y = k_{-1}/(k_1[Ba^{2+}]_o + k_{-1}) \quad (5)$$

To obtain the fraction of open channels among total channels (*Po*), the fraction of open channels in the absence of Ba^{2+} (z) was multiplied to y; z was obtained from the activation curve in the absence of Ba^{2+} (Fig. 1 *C*, *filled squares*), and it is expressed as follows:

$$z(V) = 1/(1 + \exp[(-V - 41)/8.1)] \quad (6)$$

The simulated curves of *Po* in different concentrations of Ba^{2+} are shown in Fig. 11 *A*. The effect of $[Ba^{2+}]_o$ on calculated *Po* appears to be similar to that on the voltage dependence of tail currents shown in Fig. 1 *C*. The shift of $V_{1/2}$ by increasing $[Ba^{2+}]_o$ is obtained from these curves, and the relationship is plotted as a solid line in Fig. 10 *A*. The result agrees well with the experimental data (*open squares*), suggesting that the effect of Ba^{2+} on the voltage dependence of the HERG channel results mainly from the voltage-dependent blockade.

Zn^{2+} caused faster decay. According to the result shown in Fig. 10 *B*, k_1 is about five times larger than that of Ba^{2+} (Fig. 10 *A*). The effect of the increase of k_1 by five times on the shift of $V_{1/2}$ is tested using the above model. The result is illustrated as a dotted line in Fig. 9 *A*, showing that it agrees reasonably well with the experimental data. However, the effect of Mn^{2+} on $V_{1/2}$ is more profound than expected from the above model. k_1 for Mn^{2+} is about five times smaller than that for Ba^{2+}, but $V_{1/2}$ shifts to a similar extent as Ba^{2+}. The effect of Co^{2+} and Ni^{2+} on $V_{1/2}$ is also more profound than expected, since the decay rate was not faster than Ba^{2+}, but produced larger effects on $V_{1/2}$ shift. Such discrepancy may suggest that other mechanisms are contributing to the effect of these ions on the voltage dependence of the HERG channel. In this respect, the surface charge effect should be considered in addition to the voltage-dependent blockade.

The surface charge theory was proposed to explain the channel blockade by divalent cations when it is accompanied by a shift of the voltage dependence of channel activation (Green and Andersen, 1991; Hille, 1992). The shift of gating of various ion channels has been described by the Gouy-Chapman-Stern theory (Gilbert and Ehrenstein, 1969; Hille et al., 1975; Campbell and Hille, 1976; Ohmori and Yoshii, 1977), and we used the same equation to predict the relationship between the external ionic concentration of species i (C_i) and the outer surface potential (ψ) in our experimental conditions. When the charge density remain-

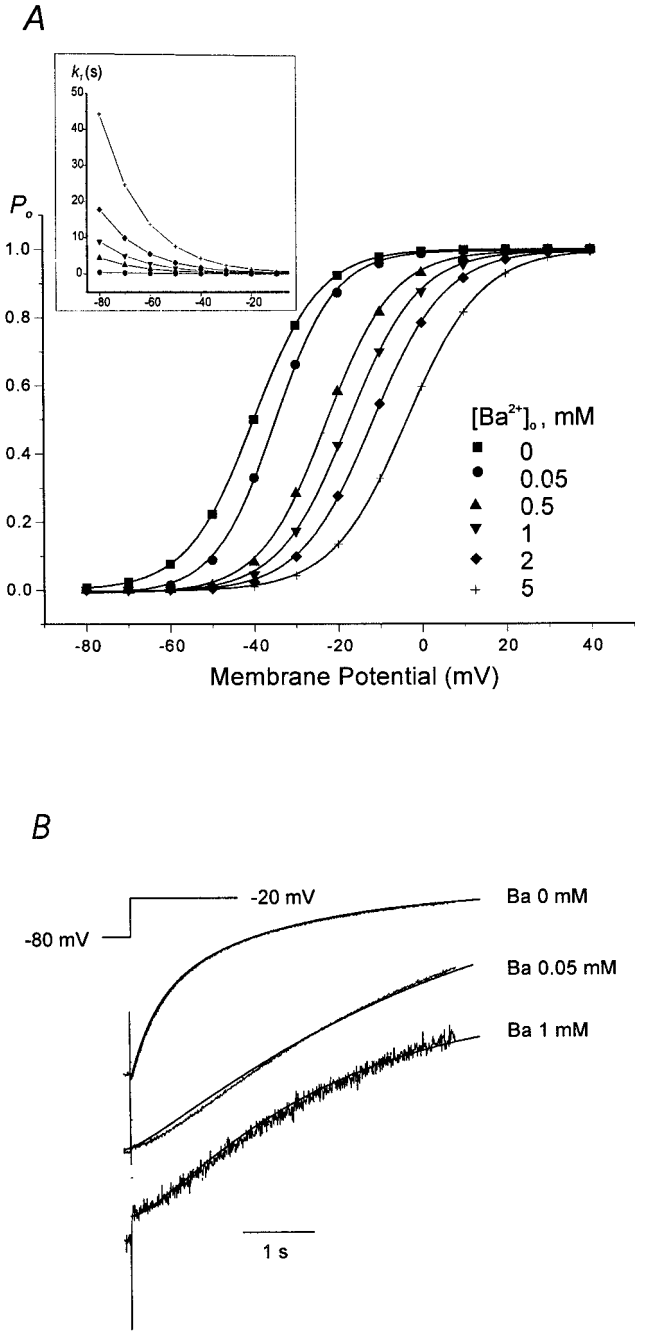

FIGURE 11 Simulation of the effect of $[Ba^{2+}]_o$ on HERG channel activation based on the voltage-dependent block model. (*A*) Simulation result of the voltage dependence of channel opening (*Po*) obtained by assuming $k_1(0)$ of 0.068. *Inset:* Rate constant of block at various $[Ba^{2+}]_o$ calculated by Eq. 3. (*B*) Superimposition of current traces and simulated results. Current traces are same as in Fig. 4 *A*. Simulated curves at 0 mM Ba^{2+}: $z(t) = 1.672 - 0.664 \exp(-t/0.378) - 0.859 \exp(-t/2.101)$. Unblock rate ($y(t)$) at 0.05 mM and 1 mM Ba^{2+} was calculated from the time constant obtained from Eqs. 3 and 4: $y(t) = 0.952 - 0.924 \exp(-t/4.315)$ at 0.05 mM. $y(t) = 0.5 - 0.499 \exp(-t/2.27)$ at 1 mM. Curves are calculated as $Po(t) = y(t) \cdot z(t)$. Current magnitude is in an arbitrary scale.

ing unneutralized in control conditions is assumed to be one negative charge per nm^2, we could obtain a theoretical curve (shown as a broken line in Fig. 9 *A*), which is reasonably close to the Sr^{2+} data. It is difficult to infer at present that this value is realistic for the HERG channel, but the previous studies for Na^+ and Ca^{2+} channels reported similar values: surface charge densities calculated from the shift of sodium channel activation by external divalent cations were $1/nm^2$ in frog nodes of Ranvier (Hille et al., 1975), and $1/0.9\ nm^2$ in the tunicate egg cell (Ohmori and Yoshii, 1977). Therefore, the shift of voltage dependency ($V_{1/2}$) by Sr^{2+} may be explained by a nonspecific charge-screening effect. In general, binding affinity of transitional metals for surface negative charge is higher than that of alkali metals, in the order of Ba^{2+}, $Sr^{2+} < Mg^{2+} < Ca^{2+} < Mn^{2+} < Co^{2+}$, $Ni^{2+} < Zn^{2+}$. So, the surface charge effect is expected to be greater for transitional metal ions, causing a greater shift of $V_{1/2}$. The result showing that transitional metal ions produce the shift of $V_{1/2}$ larger than expected from the direct channel blocking effect may well be accountable by the additional surface charge effect.

The time course of current onset is also affected by external divalent cations (Fig. 10 *B*). The effect of Ba^{2+} is remarkable, and only a low concentration (0.05 mM) causes marked slowing (Fig. 4 *A*), suggesting that the unblock rate is very slow for Ba^{2+}. This finding may suggest that Ba^{2+} binds to a site somewhere on the channel protein to stabilize a conformational state of the pore so that unblock is delayed. A sigmoid onset of current with a significant initial delay is characteristic of Ba^{2+}. To test whether such a characteristic time course is explained by the above model, we simulated the current traces in the same experimental condition shown in Fig. 4 using the simple Hodgkin-Huxley formulation. Activation at -20 mV in the absence of Ba^{2+} was well-fitted by a double-exponential function, and the effect of Ba^{2+} was reproduced by multiplying the unblock process. The result is illustrated in Fig. 11 *B*, showing a good agreement with the experimental result shown in Fig. 4 *A*. A low concentration of Ba^{2+} (0.05 mM) results in a sigmoid onset of current to a similar degree observed in the experiment. This result shows that current activation in the presence of Ba^{2+} is mainly determined by the unblock rate. On the contrary, the effect of other divalent cations on the activation kinetics differs from that of Ba^{2+}. The increase of other divalent cations caused a gradual decrease of the rate of current onset, but the slowing is not as prominent as observed in Ba^{2+}, suggesting that unblock rate is not very slow.

Another advantage of the voltage-dependent block model is to give the information about the location of the binding site in the electrical field, the so-called fractional electrical distance (δ). According to the original Woodhull's model (1973), it is represented by the voltage dependence of the dissociation constant, K_D, and can be expressed as follows:

$$K_D(E) = K_D(0) \exp(z\delta EF/RT) \qquad (7)$$

We could obtain δ of the binding site by fitting the slope of K_i in Fig. 3 *B* to Eq. 5. The slope was 15.1 mV for e-fold change. This value is not greatly different from the value

obtained from $k_1(V)$ (17 mV for e-fold change: Eq. (3)), showing a good agreement between steady-state data and kinetic data. The fractional electrical distance (δ) was calculated to be 0.64 − 0.71, suggesting that the binding site is located deep inside the channel. The voltage dependence of K_D was also obtained for other divalent cations. Mn^{2+} data (14.7 mV) in the present study (data not shown), Ca^{2+} (18.7 mV), and Mg^{2+} (15 mV) data in the previous study (Ho et al., 1998) did not show a large difference among ion species. This result may suggest that they share the same binding site. At present, however, the structural background of divalent cation binding sites of HERG channels is not known. The information about other channels that are blocked by external divalent cations in a voltage-dependent way might give some clue. Voltage-dependent block by external divalent cations was well-investigated in cyclic nucleotide-gated (CNG) channels both in functional and molecular levels. An acidic glutamate in the P region of the CNG channel (Root and MacKinnon, 1993; Eismann et al., 1994) was identified as a critical blocking site, and it was also shown that the same residue is responsible for external proton block (Root and MacKinnon, 1994). However, in the HERG gene, there is no negatively charged amino acid in the pore region (Warmke and Ganetzky, 1994). The NMDA channel is also known to be blocked voltage-dependently by external Mg^{2+} (Nowak et al., 1984; Mayer et al., 1984), and it is recently shown that substitution of asparagine residues located at the narrow constriction of the channel (especially the N + 1 site in the NR2A-subunit) strongly attenuates the block (Wollmuth et al., 1998). This possibility should be investigated in future studies.

A gating modifier theory should also be considered as a possible mechanism. This theory has been proposed to explain the effects of divalent cations when they are not sufficiently explained by surface charge theory, because activation and deactivation are not equally affected (Spires and Begenisich, 1992, 1994). This possibility cannot be excluded, but it is difficult to make a general model to test this possibility.

The three models described above mainly explain the voltage-dependent effect: shift of $V_{1/2}$ and change of kinetics. In this paper we could not propose a proper model for the decrease of maximum conductance. In the case of Ca^{2+} channel and Na^+ channels, a decrease of conductance by divalent cations was explained by the surface charge theory, since neutralizing surface negative charge by external cations can cause a decrease of the effective concentration of permeating ions near the channel pore, and thus an apparent decrease of conductance (Ohmori and Yoshii, 1977). However, the decrease of maximum conductance of HERG current cannot be explained by this theory, since HERG current was recorded as an outward current, and outward currents would not be reduced by the decrease of the effective concentration of a permeating ion from the external side of the membrane. From the result shown in Fig. 9, it was only suggested that the conductance and the voltage dependence of the HERG channel are controlled by different sites by divalent cations.

The authors thank Prof. Denis Noble for discussion and correction of English.

This work was supported by Research Grants (96-0403-01-02-2 and 97-0403-1301-5) from the Korea Science and Engineering Foundation, and the Biotech 2000 Program from the Ministry of Science and Technology.

REFERENCES

Arcangeli, A., L. Bianchi, A. Becchetti, L. Faravelli, M. Coronnello, E. Mini, M. Olivotto, and E. Wanke. 1995. A novel inward-rectifying K+ current with a cell-cycle dependence governs the resting potential of mammalian neuroblastoma cells. *J. Physiol.* 489:455–471.

Arcangeli, A., B. Rosati, A. Cherubini, O. Crociani, L. Fontana, C. Ziller, E. Wanke, and M. Olivotto. 1997. HERG- and IRK-like inward rectifier currents are sequentially expressed during neuronal development of neural crest cells and their derivatives. *Eur. J. Neurosci.* 9:1296–2604.

Armstrong, C. M. 1971. Interaction of tetraethyl-ammonium ion derivatives with the potassium channels of giant axon. *J. Gen. Physiol.* 58: 413–437.

Bianchi, L., B. Wible, A. Arcangeli, M. Taglialatela, F. Morra, P. Castaldo, O. Crociani, B. Rosati, L. Faravelli, M. Olivotto, and E. Wanke. 1998. Herg encodes a K^+ current highly conserved in tumors of different histogenesis: a selective advantage for cancer cells? *Cancer Res.* 58: 815–822.

Brown, H. F., A. Clark, and S. J. Noble. 1976. Analysis of pacemaker and repolarization currents in frog atrial muscle. *J. Physiol. (Lond.).* 258: 547–577.

Brown, H. F., and D. DiFrancesco. 1980. Voltage clamp investigations of membrane currents underlying pacemaker activity in rabbit sinoatrial node. *J. Physiol. (Lond.).* 308:331–351.

Campbell, D. T., and B. Hille. 1976. Kinetics and pharmacological properties of the sodium channel of frog skeletal muscle. *J. Gen. Physiol.* 67:309–323.

Eismann, E., F. Muller, S. H. Heinemann, U. B. and Kaupp. 1994. A single negative charge within the pore region of a cGMP-gated channel controls rectification, Ca2+ blockage, and ionic selectivity. *Proc. Natl. Acad. Sci. USA.* 91:1109–1113.

Faravelli, L., A. Arcangeli, M. Olivotto, and E. Wanke. 1996. A HERG-like K+ channel in rat F-11 DRG cell line: pharmacological identification and biophysical characterization. *J. Physiol.* 496.1:13–23.

French, R. J., and J. J. Shoukimas. 1985. An ion's view of the potassium channel. The structure of the permeation pathway as sensed by a variety of blocking ions. *J. Gen. Physiol.* 85:669–698.

Gilbert, D. L., and G. Ehrenstein. 1969. Effect of divalent cations on potassium conductance of squid axons: determination of surface charge. *Biophys. J.* 9:447–463.

Green, W. N., and O. S. Andersen. 1991. Surface charges and ion channel function. *Annu. Rev. Physiol.* 53:341–359.

Hagiwara, S., S. Miyazaki, W. Mooky, and P. Patlak. 1978. Blocking effects of barium and hydrogen ions on the potassium current during anomalous rectification in the starfish egg. *J. Physiol.* 279:167–185.

Hille, B. 1992. Ionic Channels of Excitable Membranes. Sinauer Associates Inc., Sunderland, MA.

Hille, B., A. M. Woodhull, and B. I. Shaprio. 1975. Negative surface charge near sodium channels of nerve: divalent ions, monovalent ions, and pH. *Phil. Trans. R. Soc. Lond. B.* 270:301–318.

Ho, W.-K., Y. E. Earm, S. H. Lee, H. F. Brown, and D. Noble. 1996. Voltage- and time-dependent block of delayed rectifier K^+ current in rabbit sino-atrial node cells by external Ca^{2+} and Mg^{2+}. *J. Physiol.* 494:727–742.

Ho, W.-K., I. Kim, C. O. Lee, and Y. E. Earm. 1998. Voltage-dependent blockade of HERG expressed in Xenopus oocytes by external Ca^{2+} and Mg^{2+}. *J. Physiol.* 507.3:631–638.

Irisawa, H., H. F. Brown, and W. Giles. 1993. Cardiac pacemaking in the sinoatrial node. *Physiol. Rev.* 73:197–227.

Mayer, M. L., G. L. Westbrook, and P. B. Guthrie. 1984. Voltage-dependent block by Mg^{2+} of NMDA responses in spinal cord neurones. *Nature*. 309:261–263.

Noble, D., and R. W. Tsien. 1969. Outward membrane currents activated in the plateau range of potential in cardiac Purkinje fibers. *J. Physiol. (Lond.).* 200:205–231.

Nowak, L., P. Bregestovski, P. Ascher, A. Herbet, and A. Prochiantz. 1984. Magnesium gates glutamate-activated channels in mouse central neurons. *Nature.* 307:462–465.

Ohmori, H., and M. Yoshii. 1977. Surface potential reflected in both gating and permeation mechanisms of sodium and calcium channels of the tunicate egg cell membrane. *J. Physiol.* 267:429–463.

Root, M. J., and R. MacKinnon. 1993. Identification of an external divalent cation-binding site in the pore of a cGMP-activated channel. *Neuron*. 11:459–466.

Root, M. J., and R. MacKinnon. 1994. Two identical noninteracting sites in an ion channel revealed by proton transfer. *Science*. 265:1852–1856.

Sanguinetti, M. C., C. Jiang, M. E. Curran, and M. T. Keating. 1995. A mechanistic link between an inherited and an acquired cardiac arrhythmia: *HERG* encodes the I_{Kr} potassium channel. *Cell*. 81: 299–307.

Sanguinetti, M. C., and N. K. Jurkiewicz. 1991. Delayed rectifier outward K+ current is composed of two currents in guinea pig atrial cells. *Am. J. Physiol.* 260:H393–H399.

Shibasaki, T. 1987. Conductance and kinetics of delayed rectifier potassium channels in nodal cells of the rabbit heart. *J. Physiol.* 387:227–250.

Smith, P. L., T. Baukrowitz, and G. Yellen. 1996. The inward rectification mechanism of the HERG cardiac potassium channel. *Nature*. 379: 833–836.

Spector, P. S., M. E. Curran, A. Zou, M. T. Keating, and M. C. Sanguinetti. 1996. Fast inactivation causes rectification of the I_{Kr} channel. *J. Gen. Physiol.* 107:611–619.

Spires, S., and T. Begenisich. 1992. Chemical properties of the divalent cation binding site on potassium channels. *J. Gen. Physiol*. 100: 181–193.

Spires, S., and T. Begenisich. 1994. Modulation of potassium channel gating by external divalent cations. *J. Gen. Physiol.* 104:675–692.

Standen, N. B., and P. R. Stanfield. 1978. A potential- and time-dependent blockade of inward rectification in frog skeletal muscle fibres by barium and strontium ions. *J. Physiol.* 280:169–191.

Trudeau, M. C., J. W. Warmke, B. Ganetzky, and G. A. Robertson. 1995. HERG, a human inward rectifier in the voltage-gated potassium channel family. *Science*. 269:92–95.

Wang, S., S. Liu, M. J. Morales, H. C. Strass, and R. L. Rasmusson. 1997. A quantitative analysis of the activation and inactivation kinetics of *HERG* expressed in *Xenopus* oocytes. *J. Physiol.* 502.1:45–60.

Warmke, W. W., and B. Ganetzky. 1994. A family of potassium channel genes related to eag in Drosophila and mammals. *Proc. Natl. Acad. Sci. USA.* 91:3438–3442.

Wollmuth, L. P., T. Kuner, and B. Sakmann. 1998. Adjacent asparagines in the NR2-subunit of the NMDA receptor channel control the voltage-dependent block by extracellular Mg^{2+}. *J. Physiol.* 506.1:13–32.

Woodhull, A. M. 1973. Ionic blockage of sodium channels in nerve. *J. Gen. Physiol.* 61:687–708.

Wymore R. S., Gintant, G. A., Wymore, R. T., Dixon, J. E., McKinnon, D. and Cohen, I. S. 1997. Tissue and species distribution of mRNA for the I_{Kr}-like K^+ channel, erg. *Circ. Res.* 80:216–268.

Zou, A., M. E. Curran, M. Keating, and M. C. Sanguinetti. 1997. Single HERG delayed rectifier K+ channels expressed in Xenopus oocytes. *Am. J. Physiol.* 272:H1309–H1314.